

## **Studying the Effect of Punch Nose Radius on Deep Drawing Operation**

\*Dr. Waleed K. Jawad

\*Jamal H. Mohamed

**Received on: 23/11/2005**

**Accepted on: 27/4/2006**

### **Abstract:**

This work aims to study the effect of varying punch nose radius used in deep drawing operation, on produced cup wall thickness, stress and strain distribution across the wall of the drawn part, hydrostatic pressure, residual stress developed in the drawing part after drawing, and the value of work done to form the required shape of drawn part.

In this work, six types of punches with various nose radii have been used to form a cylindrical cup of (44mm) outer diameter, (28mm) height, and (0.5mm) sheet thickness of mild steel of (0.15%) carbon content. A commercially finite element program code (ANSYS 5.4), was used to perform the numerical simulation of the deep drawing operation, and the numerical results were compared with the experimental work.

The results show that, the value of work required to form parts with large nose radii is much more than the value required to form parts with small punch nose radii. An increase in the punch nose radius, results in an insignificant increase in shear stress and shear strain. These values are very small which can be ignored.

The greatest thinning is seen to occur with hemispherical punch (Dome shaped punch) due to great stretching of the metal over the punch head. The maximum tensile stresses and the maximum thinning of the dome wall occur nearly at the apex of the dome (a friction coefficient nearly equal to zero). In the presence of friction, the position of maximum strain, which corresponds to the location of maximum thinning point, moves away from the apex. The larger the friction is, the larger is the distance between the apex and the point of maximum thinning. The frictional force is applied to the metal largely by the edge of the punch and not by its flat section. Maximum thickening of the cup wall occurs at the flange rim, and this thickening increases with punch stroke.

\*Dept. of Production eng., Univ. of Tech.

**الخلاصة:**

يهدف هذا البحث إلى دراسة تأثير التغير في نصف قطر استدارة مقدمة المخرم في عملية السحب العميق على كل من، سمك الجدار للقدح المنتج، وتوزيع الأجهادات والانفعالات الموقعية، وتوزيع الأجهادات والانفعالات القصية والاجهادات المتبقية (residual stresses) و (hydrostatic pressure) على جدار القدح المنتج، ومقدار الشغل اللازم لتشكيل الجزء المسحوب. في هذا العمل، تم إنتاج قدح أسطواني بقطر خارجي (44 mm) وبارتفاع (28 mm) من صفيحة سمكها (0.5 mm) من معدن الصلب الطري (mild steel) ذو نسبة كربون (0.15 %). حيث تم استخدام ستة مخارم بقطر (43 mm) نوات أنصاف أقطار مقدمة (P=3,6,9,15,18,&21.5mm) لغرض استخدامها في الجزء العملي. أما نصف قطر استدارة مقدمة القالب الأنثى فقد تم تثبيته على (P =6mm). تم استخدام برنامج (ANSYS 5.4) الخاص بتقنية العناصر المحددة في تمثيل عملية المحاكات للسحب العميق، مع مقارنة النتائج العملية والنظرية.

وقد أثبتت النتائج أن الشغل اللازم لتشكيل الأقداح ذات أنصاف أقطار الاستدارة الكبيرة لمقدمة المخرم، يكون أكبر بكثير من الشغل اللازم لتشكيل الأقداح ذات أنصاف أقطار الاستدارة الصغيرة. كما أن التغير في نصف قطر استدارة مقدمة المخرم لا يؤثر على قيمة إجهادا وانفعالات القص، وان هذه القيم صغيرة جدا يمكن إهمالها. أن أكبر تخفيف لسمك الجدار في القدح المنتج يحدث عند استخدام المخارم ذات الرأس الكروي (Dome shaped punch)، بسبب حالة المط المفرد تحت رأس المخرم. كما ان أقصى إجهاد سحب وأقصى تخفيف في سمك الجدار يحدث تقريبا عند مقدمة الرأس الكروي (apex of the dome) (في حالة الاحتكاك القليل جدا) أما في حالة وجود الاحتكاك، فان موقع أقصى انفعال والذي يقابله موقع أكبر تخفيف في السمك سوف يبتعد قليلا عن مقدمة رأس المخرم، حيث كلما زاد الاحتكاك كلما بعدت النقطة التي تمثل أقصى تخفيف في السمك عن قمة المخرم. كذلك وجد أنه لجميع المخارم المختارة أن قوة الاحتكاك تتركز عند الحافة المقوسة للمخرم وليس على الوجه المستوي له. كما أن أقصى زيادة في سمك الجدار تحدث عند حافة القدح، وهذه الزيادة في سمك الجدار تزداد مع زيادة طول الشوط.

**Introduction:**

Deep drawing is one of the most important processes for sheet metal forming. It is the best for the mass production of part pieces for many different applications, such as lighter casing or part of automobile bodies. Deep drawing may be defined as the process in which a blank or workpiece, usually controlled by a pressure plate, is forced in to and /or through a die means of a punch to form a hollow component in which the thickness is substantially the same as that of the original material.

Since a number of investigators have studied the drawing process, the current exposition here will focus only on the researches concerning the use of Finite Element Method (FEM) in deep-drawing process .

In (1994), Danckert [1], proposed a finite element simulation of two stage deep drawing process followed by ironing of the cup wall to analyze the residual stresses in the cup wall after the drawing stages and after ironing of steel blank .The results show that the ironing process causes a drastic change in the residual stress and causes a distribution which is favorable with regard to fatigue strength, stress corrosion resistance and stress cracking.

Iwata et al. (1995) [2,3], have present two papers, the first one [2], concerns a theoretical approach to discuss the constitutive equations for 3D analysis of sheet metal forming. Further it has been found that the breakage could be predicted using the idea that localized necking directly induces breakage of sheet. In the second paper [3], a square cup deep-drawing process is numerically

simulated by elastic-plastic FEM. Friction coefficients on dies are measured, and the actual pressure distribution on the blank-holder is taken into account in the calculation. They have concluded that the site of fracture initiation is almost coincident with that at which sheet thickness is most reduced.

Suri & Otto (1998) [4], have described algorithms developed to predict wall thickness profiles for two different cup geometries (straight-walled & tapered cup), and then compared these predictions with measured value from aluminum and steel cups drawn in the laboratory. The results show that the model is robust to friction for the straight-walled cup, indicating that errors in frictional coefficient will not greatly alter the predictions. While in tapered cup, the errors indicate that the actual friction coefficient during forming was close to the theoretical value used.

Yao et al. (2000) [5], proposed a modified axisymmetric model with a center offset to predict tearing failure in the corner section of 3D parts. The proposed offset was found to be a function of the failure height, process parameters, including tooling geometry, material properties, friction coefficient, and restraining force provided by the blank holder .

FE modeling proposed by Altan (2000) [6], for the Limiting Dome Height (LDH) test shows that this test is very sensitive to friction. The results show that, the presence of friction, however hinder the free thinning at the apex of the punch. Therefore, the position of maximum

strain, which corresponds to the location of maximum thinning point moves away from the apex. The larger the friction, the larger the distance between the apex and the point of maximum thinning.

Wang & Cao (2000)[7], have developed an analytical approach to calculate the critical wrinkling condition under a constant binder force and pressure. It was found that the material strain hardening exponent along with binder pressure has a significant effect on the critical buckling stress as well as the buckling mode.

In the paper of Lee & Cao (2001)[8], an axisymmetric shell element for the multi-step inverse analysis is developed for more accurate prediction of design variables such as the initial blank shape, strain distribution, and intermediate shapes. The results show that as the number of analysis steps is increased, this approach is more accurate and the punch increment per step is much larger than that in the conventional incremental analysis.

Hun & Kim (2001)[9], have applied inverse FE analysis to estimate the initial blank shape, intermediate deform shape, thickness distributions and failure during multistage deep drawing operation of elliptic cup. The results show that the localized deformation occurs along the major axis of the elliptic cup and the wrinkling occurs along the minor axis, the modified design improves the quality of drawn part and reduce the possibility of failure occurrence.

#### **Theoretical Finite Element Procedure:**

where:  $\{R\}$  is the nodal force ,  
 $\{dU\}$  is the incremental displacement  
,  $[K (dU)]$  is the system stiffness  
matrix, and can be expressed in terms

Seao (2002)[10], have used FEM to foresee the defects occurring during deep drawing operation such as wrinkling, thinning, and fracture; and how to prevent their occurrence during production through simple design changes. It was found that, because the die radius and the clearance were relatively small, the material around the wall experienced excessive compressive stress rather than just being pulled in to the die.

Ahmed et al. (2004)[11], have proposed finite element simulation of axisymmetric sheet forming operations to predict the strain variation and the deformation history of axisymmetric sheet forming operation.

Singh & Kumar (2005) [12], investigated the construction of cylindrical cup of low carbon steel by using hydromechanical deep drawing process. It was found that, by hydromechanical deep drawing, higher drawability and more uniform thickness distribution could be obtained when compared to conventional deep drawing.

Abedrabbo & Zampaloni (2005)[13]. investigated the wrinkling behavior of aluminum alloys during hydroforming process, when using square and round blank. It was found, that in the case of square blank, wrinkles do not form underneath the blank holder, as rigid corners prevent drawing and cause the sheet to stretch. On the other hand, wrinkling is prevalent the case of round blank, as the metal draw easily into the die cavity creating large compressive stress in the flange region.

The nonlinear finite-element equation is expressed as follows:

$$[K (dU )]\{dU\} = \{R\} \text{-----} 1$$

Using Equ. (2) ~ (5) and the left side of Equ. (1), the following relationship between the nodal force and the incremental displacement (dU) can be obtained.

$$\begin{aligned}
 [K (-dU)]\{-dU\} &= \Sigma [B]^T [D (-dU)]\{B\}v \{-dU\} \\
 &= \Sigma [B]^T [D (dU)]\{B\}v \{-dU\} \\
 &= -[K (dU)]\{dU\} \\
 &= -\{R\}
 \end{aligned}$$

Equation (6) satisfies the condition that the nodal force reverses when the incremental displacement reverse.

It is assumed that coulomb friction acts over the top and bottom surface of the flange. In practice, the cup wall will be drawn in the presence of a blank holder, but this does not negate the assumption of plane stress over the major portion of the flange in the finite element calculations of the preceding article. The normal stresses created by the blank holder are usually quite small compared to  $(\sigma_y)$ , of the material. Since the assumption of the plane stress is not satisfied by the analysis during the early stages of flange deformation, we assume that blank holder force is centered at the nodal point of the finite element. The components of the nodal frictional force  $(R_{fx}, R_{fy})$  are assumed to act in the plane of the flange and are calculated from :

$$\begin{pmatrix} R_{fx} \\ R_{fy} \end{pmatrix} = \frac{-2\mu H_w}{(dU_{fx}^2 + dU_{fv}^2)^{1/2}} \begin{pmatrix} dU_{fx} \\ dU_{fv} \end{pmatrix} \tag{7}$$

of the stress-incremental strain matrix [D], the [B] matrix and the volume of the element (v) as:

$$[K (dU)] = \Sigma [B]^T [D (dU)]\{B\}v \tag{2}$$

If the deformation in the flange is one of plane stress and assuming the material is rigid perfectly plastic and obeys the von Mises yield criterion, the [D] matrix can be expressed as follows (14) [1995]:

$$[D] = \frac{4\sigma_y}{3d\epsilon_{eq}} \begin{vmatrix} 1 & 1/2 & 0 \\ 1/2 & 1 & 0 \\ 0 & 0 & 1/4 \end{vmatrix} \tag{3}$$

where:

$\sigma_y$  is the yield stress,  $d\epsilon_{eq}$  is the equivalent plastic strain increment, where :

$$\sigma_y = \left( \sigma_x^2 + \sigma_y^2 + 3\tau_{xy}^2 \right)^{1/2} \tag{4}$$

and

$$d\epsilon_{eq} = (2/\sqrt{3}) \left( d\epsilon_x^2 + d\epsilon_y^2 + d\gamma_{xy}^2/4 \right)^{1/2} \tag{5}$$

**Numerical Simulation :**

A cup of (44mm) outer diameter, and (28mm) height, was chosen for detailed analysis of deep drawing operation. The blank from which it is formed has a diameter of (82mm), (0.5mm) thickness and is comprised of mild steel of 0.15% carbon content, (200MPa) yield stress, (200GPa) Modulus of elasticity, (0.5GPa) Tangent modulus and of (0.3) Poisson’s ratio.

A commercial FE code (ANSYS 5.4) was used to simulate the deep drawing operation. Elasto-plastic behavior for work material was used in the simulation. The blank material was modeled with (Visco106 element).It is assumed that the punch, the die and the blank holder are rigid and are represented by(solid element 42). The contact interface between the die and the deformed material is represented by (contact element 48). A Coulomb friction law was employed to investigate the effect of friction at the tool–material interface ( $\mu=0.1$ ). The blank holding force was ranging from (10-15KN) during the full stroke of operation. The clearance between punch and die was set to be (1.1 sheet thickness). A successive stages of the deep drawing sheet for varying punch stroke are shown in fig. (1).

**Experimental Work:**

In this work, a deep drawing tooling was designed and constructed to carry out the experimental work as shown in fig. (2). Six types of punches of (43mm) diameter with punch nose radii of {P=3,6,9,15,18, & 21.5 mm (Dome shape punch)} were used, and the value of die nose radius is kept constant to (d = 6mm).

Where ( $\mu$ ) is the coefficient of coulomb’s friction, the quantities  $dU_{fx}$  and  $dU_{fy}$  are the incremental displacement components, and  $H_w$  is the blank holder force at each nodal point calculated in the finite element program.

From eq. (7). It can be determined that :

$$\{R_f(-dU)\} = \{R_f(dU_f)\} \text{-----} \\ \text{-----} 8$$

Hence Eq. (8) satisfies the requirement that the friction force reverses when the incremental displacement reverses at the normal point.

The incremental thickness change ( $\Delta t$ ) of flange thickness ( $t$ ) is expressed in the finite element method as follows:

$$\Delta t = dC_t t \\ = -(dC_x + dC_y)t \\ = -[B]t\{dU^e\} = 0 \text{-----} \\ \text{-----} 9$$

However, we set  $\Delta t = 0$ , and neglect the effect of thickness change in order to simplify the complicated calculation for the multi objective optimization problem (optimum –shaped blank and limiting size of blank)

A study of the bending and unbending as the material passes over the die radius has been conducted by many investigators. For example a simple model adopted by Siebel & Beisswanger (1992) [15], mentions that the nodal force ( $H_b$ ) based on the bending at the die radius is expressed as:

$$H_b = [1 + \exp(\pi\mu / 2)] t^2 L\sigma_y / \\ [4(\rho_d + t / 2) \text{-----} 10$$

where : (L) and ( $\rho_d$ ) denote the circumferential length of the inner boundary and radius, respectively.

$$[\text{Hoop strain}] \quad \epsilon_h = -(\epsilon_r + \epsilon_t)$$

$$[\text{Effective strain}] \quad \epsilon_{\text{eff}} = \{2/3 (\epsilon_r^2 + \epsilon_t^2 + \epsilon_h^2)\}^{0.5}$$

Where :

(to) is the initial thickness of the blank (0.5 mm).

( t ) is the final thickness of produced cup wall (mm).

(Lo) is the initial radius of the grid circle printed on the blank (mm).

(L) is the average of final radius of the grid circle after deformation (mm).

(ΔL) is the changes in radius of grid circle after deformation.

$$\text{Where, } L = L_o + \Delta L$$

**Results and Discussion:**

FE Modeling of deep drawing operation at varying punch strokes is shown in fig. (3), It is shown obviously that relatively high stress concentration occurs at the die corner radius as a result of excessive bending of material. The material lying under the flat punch is more constrained, and therefore deformed less. Localized thinning occurred near to the punch corner. This mean that frictional force is applied to the metal largely by the edge of the punch and not by its flat section. Therefore, it has been assumed that friction force is present wherever there is a curvature on the surface of the drawn part.

It is seen from fig. (3), that for dome shape punch (P=21.5 mm), the maximum thinning of the dome wall occurs nearly at the apex of the dome. This is because, in the absence of friction (a friction coefficient nearly equal to zero), the maximum tensile stresses occur at the apex,

The experiments were carried out using the Instron testing machine which has a capacity of 100KN and cross head speed of (300mm/min), with punch stroke ranging from (35-40mm). The material properties are the same as that mentioned before in section of the numerical simulation.

In order to study the strain distribution within the cup during drawing operation, a grid pattern of (5, 10, 15,20, 25, 30, 35& 40) mm radius circles, was chosen and printed (along 12 intersecting chosen lines, 30 degree apart) on the original blank, by using mechanical grid marker. In order to measure the cup wall thickness at the deformed grid circle after drawing; the drawn cup was divided in to two parts (to facilitate the thickness measuring process of the cup wall) by using a diamond saw as shown in fig. (2). Digital thickness micrometer was used to measure the produced cup wall thickness (t) after drawing, and tool microscope was used to measure the final radius of grid circle (L) at the cup wall after drawing. The thickness and average final radius of grid circle were measured along the 12 intersecting lines as shown in fig (2).

Experimentally, the radial strain (εr) was obtained by measuring the final radius of the distorted grid circle after deformation (L). The thickness strain (εt) was obtained by measuring the final cup wall thickness (t) at the deformed grid circle (along the12 intersecting lines). Slab method was used to calculate these strains as follow :

$$[\text{Radial strain}] \quad \epsilon_r = \ln (L / L_o)$$

$$[\text{Thickness strain}] \quad \epsilon_t = \ln ( t / t_o)$$

thickness in the wall and flange regions. At the punch nose (necking point), there is a small tension which causes thinning of initial blank thickness to about (5-7)%, and afterward it become compression which causes thickening of the cup wall.

In our case, the flange rim (edge of the produced cup) undergoes the most severe shrinking during the process, and hence becomes the thickest part of the flange. That is why the horizontal restraining force resulting from the friction between the die / blank holder and the blank are sometimes considered as being applied at the flange rim. This can be shown obviously by thickening of the cup wall at the flange rim to about (20-25 %) theoretically (FEM) & (17-22%) experimentally.

For large value of punch nose radii {P=15,18& 21.5mm (dome shape punch)} the material lying at the punch region is deforms more than the other portion of the cup wall and produces more thinning leading to high stress concentration at the punch nose radius as a result of excessive bending and stretching of metal at the punch head. It is seen obviously that the thinning increases with increasing punch nose radius, and maximum thinning occurred at the largest punch nose radius value punch stroke influences greatly the wall thickness and strain values, in which these values increases with stroke increasing. It is seen that necking (Max thinning), occurs at the punch nose region for all strokes, and thickening of flange rim, increases with punch stroke due to excessive shrinking of flange. These values of effective stress is decreases with stroke increasing, due to the fact that, at punch strokes more than 20mm,

thus making the sheet to thin out gradually toward the apex. In the presence of friction, however free thinning at the apex of the punch is hindered, therefore the position of maximum strain, which corresponds to the location of maximum thinning point moves away from the apex. The larger is the friction, the larger is the distance between the apex and the point of maximum thinning. This explanation give good agreements with FE modeling proposed by Altan [Ref.6].

Thickness along the grid circles at the produced cup wall was measured and the percentage change of thickness was calculated and compared with change in thickness obtained by simulation as shown in fig. (4). It is clear from the figure, that initial blank thickness (0.5mm) at the region of a flat bottom face of the small punch nose radii (P=3,6,&9mm), does not change and remains almost constant. This is because, the flat face of the punch is in contact with blank, and due to the drawing force, friction comes into play, which prevents any deformation of the metal under the punch. Hence there is no thickness change observed at this region. However, the necessary deformation is provided by other portions of the cup, resulting in an increase of (P=21.5mm dome shape punch).The amount of thinning reach to about (12,18,&27)% theoretically, and (10,15,&18)% experimentally, for large punch nose radii of (P= 15,18, & 21.5 mm) respectively.

Fig. (5) show the effect of punch stroke (punch displacement) on cup wall thickness, effective (equivalent) strain, and effective stress, for punch nose radii equal to (P=3&21.5mm). It is clear that the

increase in the maximum strain at the flange rim. It is shown obviously that the more uniform distribution the more reasonable values of strain is for the value of punch nose radius of ( $P=3,6\text{mm}$ ), i.e. when the value of punch corner radius is equal to (6-12) times the sheet thickness, which give good agreement with practical application.

The effect of punch nose radius on shear strain and shear stress distribution can be readily deduced from fig. (8). It is noted from the figure, that an increase in the punch nose radius, results in an insignificant increase in shear stress or shear strain. The nature of the shear strain ( $\epsilon_{xy}$ ) and shear stress ( $S_{xy}$ ) are almost tensile with small value at the cup bottom and increase toward the cup wall, and reaches its maximum value at the cup rim. These values of stresses are very small (between 10-17 MPa) for all geometries chosen, which can be ignored. (*It was found* theoretically (FEM), that the value of shear strains ( $\epsilon_{xy}$  &  $\epsilon_{yz}$ ) and shear stresses ( $S_{xz}$  &  $S_{yz}$ ) are equal to zero).

Fig. (9) show the distribution of residual stress developed in the cup after drawing for all punch geometries chosen. It is evident that the stress increasing toward the cup rim, and the trend of the curves are the same, but the die with punch nose ( $P=6\text{mm}$ ) has a lower residual stress and more uniformly distributed than the other geometries.

The hydrostatic pressure distribution over the cup wall caused by the residual stresses after drawing is shown in fig. (10). It evident that the hydrostatic pressure for punch nose ( $P=6\text{mm}$ ) is always positive and much more uniformly distributed than the other geometries.

the flange starts to leave the blankholder, and there fore reducing greatly the restraining forces applied to the metal, which cause the metal to form freely with minimum force.

Fig. (6) show a comparison between calculated strains ( $\epsilon_r, \epsilon_t, \epsilon_h,$  &  $\epsilon_{eff}$ ) obtained from experimental work, and predicted values obtained from the simulation for completely drawn part for all punches chosen. It is clear that a considerable change of the strain distribution is observed in the flat as well as radius areas of the punch. The material lying on the small punch nose radii ( $P=3,6,9\text{ mm}$ ) is more constrained, and therefore deforms less. However, since the final configuration is fixed, the necessary deformation is provided by other portions of the cup, resulting in an increase of strain in the wall and flange region of the drawn part. It is clear from these figures that the strain distributions of all geometries chosen are similar in shape, and have the same trend and approximately the same values, except for the large nose radii ( $P=15,18,&21.5\text{mm}$ ), where high strain concentration are present at the punch nose as a result of excessive stretching of metal over the punch nose. It seen from these figures, that the experimental values of strains are lower than the theoretical values (FEM), this may be due to the lack of exact information about material properties or friction condition.

Fig.(7) show a comparison between calculated effective strain obtained from experimental work and theoretically (FEM) for different values of punch corner radii of completely drawn part. It is noted that an increase in the punch nose radius results in an insignificant

than the other portion of the cup wall and produces more thinning and high stress concentration at the punch nose. It is seen obviously that the work required to form apart with large nose radii are much more than small nose radius.

By returning to figures (4,6,7,9,11), one can conclude that, the more uniform distribution of cup wall thickness, the more reasonable and smallest values of stress, strain and work done are for the value of punch nose radius equal to ( $P=6$  mm). Since the

the give good agreement with practical application.

### **Conclusions:**

maximum thinning of the dome wall occurs nearly at the apex of the dome. The larger is the friction, the larger is the distance between the apex and the point of maximum thinning. The more uniform distribution the more reasonable and smallest values of stress, strain and work done are for the value of punch nose radius equal to (12 times sheet thickness).

Because a positive hydrostatic pressure near the cup wall will reduce the tendency to crack formation, increase the load that the cup wall can sustain before cracks are formed, increase the fatigue life and strength of the cup wall and increase the corrosion resistance of the cup wall (Ref.1), one can conclude that punch nose radius ( $P=6$  mm) is more convenient for drawing condition of this research.

Fig. (11) show the effect of punch nose radius on work done distribution. Since the material lying at the punch nose is deforms more initial blank thickness equal to (0.5mm), this mean that the best punch nose radius is equal to (12times blank thickness), which

In summary, we can conclude that frictional force is applied to the metal largely by the edge of the punch and not by its flat section. For all punch geometries chosen, necking (maximum thinning of the cup wall) occurs at the punch nose, thickening of the cup wall occurs at the flange rim and increasing with punch stroke, the value of shear stress ( $S_{xy}$ ) and shear strain ( $\epsilon_{xy}$ ) are very small which can be ignored. The value of work required to form apart with large nose radius are much more than the value required to form apart with small punch nose radius.

For dome shape punch, the maximum tensile stresses and

**References:**

- [1]- .Danckert ,J “The residual stress distribution in the wall of a deep drawing and ironed cup determined experimentally and by finite element method” , Annals of the CIRP, vol43 ,(1994).
- [2]-.Iwata,M;Gotoh,M & Matsui, “Finite element simulation of deformation and breakage in sheet metal forming (1<sup>st</sup> report, Basic theory)”, JSME International Journal, Series A, vol.38,(1995), p.281-287.
- [3]-.Iwata,N;.Gotoh,M & Goth,M “Finite element simulation of deformation and breakage in sheet metal forming,(2<sup>nd</sup> report, An elastic-plastic Analysis of square-cup drawing process)” , JSME International Journal series A , vol 38, N2, (1995),p.289-295.
- [4].Suri,R & Otto,K.N “Models to integrate sheet metal part and process design”, International Seminar On Manufacturing System, (1998),p.1-6.
- [5]-Yao,H;.Kinsey,B.L & Cao,I Rapid design of corner restraining force in deep drawn rectangular parts, International Journal of Machine Tools and Manufacture ,(2000),p.113-131.
- [6]-.Altan,T “A practical approach to evaluate friction”, Stamping Journal, (2000),p.80-81
- [7] .Wang -Xi & Cao, J. “An analytical prediction of flange wrinkling in sheet metal forming”, Journal of Manufacturing Processes, vol.2 / No2,(2000),p.100-107.
- [8]- .Lee C & Cao J,“Shell element formulation of multi-step inverse analysis for axisymmetric deep drawing process”, Int.J.Numer.Meth.Engng, vol 50,(2001),p.681-706.
- [9]-.Hun,H & .Kim,S “Process design for multi-stage elliptic cup drawing with the large aspect ratio”, Journal of material processing technology,vol 113,(2001),p.779-785.
- [10]-.Seao,Y“Simulation beats trial and error”, Metal forming magazine, (www.metal forming magazine.com), (2002).
- [11]-.Ahmed.,M; Sekon.,S.G & .Singh,D “Finite element simulation of axisymmetric sheet forming operations using shell element”, (2000), (Internet).
- [12]-.singh,S.K & Kumar, “ Numerical prediction of limiting drawing ratio and thickness variation in hydromechanical deep drawing”,INDER Science, [www.inderscience.com](http://www.inderscience.com), copyright (2005),Int.
- [13].Abedrabbo,N.&Zampaloni,M.A “Wrinkling control in aluminum sheet hydroforming”, International journal of mechanical science.Vol.47 (2005)p.333-358.
- [14]-.Iseki., & .Sowerby,R“Determination of the optimum blank shape when deep drawing nonaxisymmetric cups, using a finite element method” JSME International Journal, series A, Vol38,No4,1995.

[15]-Iseki,H. & .Sowerby,R  
;Murota,R & Takahashi,K  
“The limiting drawing ratios  
of optimum blank shapes”  
Trans.Jpn.Soc.Mech.Eng,  
Vol58,No548,p1327,1992.

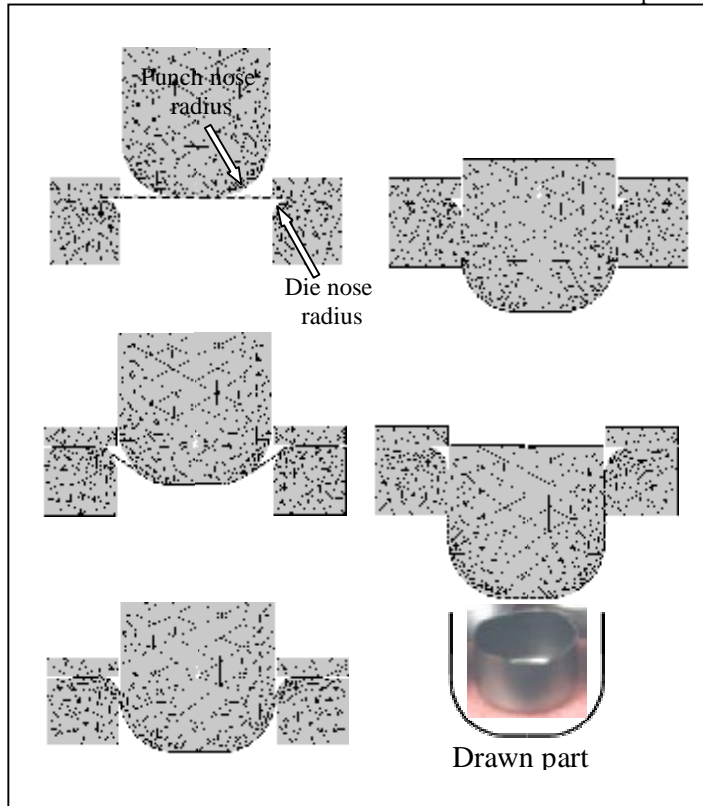


FIG ( 1 ) : A successive stages of deep drawing operation using Finite Element Simulation for varying punch strokes.



FIG ( 2 ) : Drawing die used in the experimental work, completely drawn parts (produced cup) , divided part & the distortion of grid circles at the cup wall & bottom.

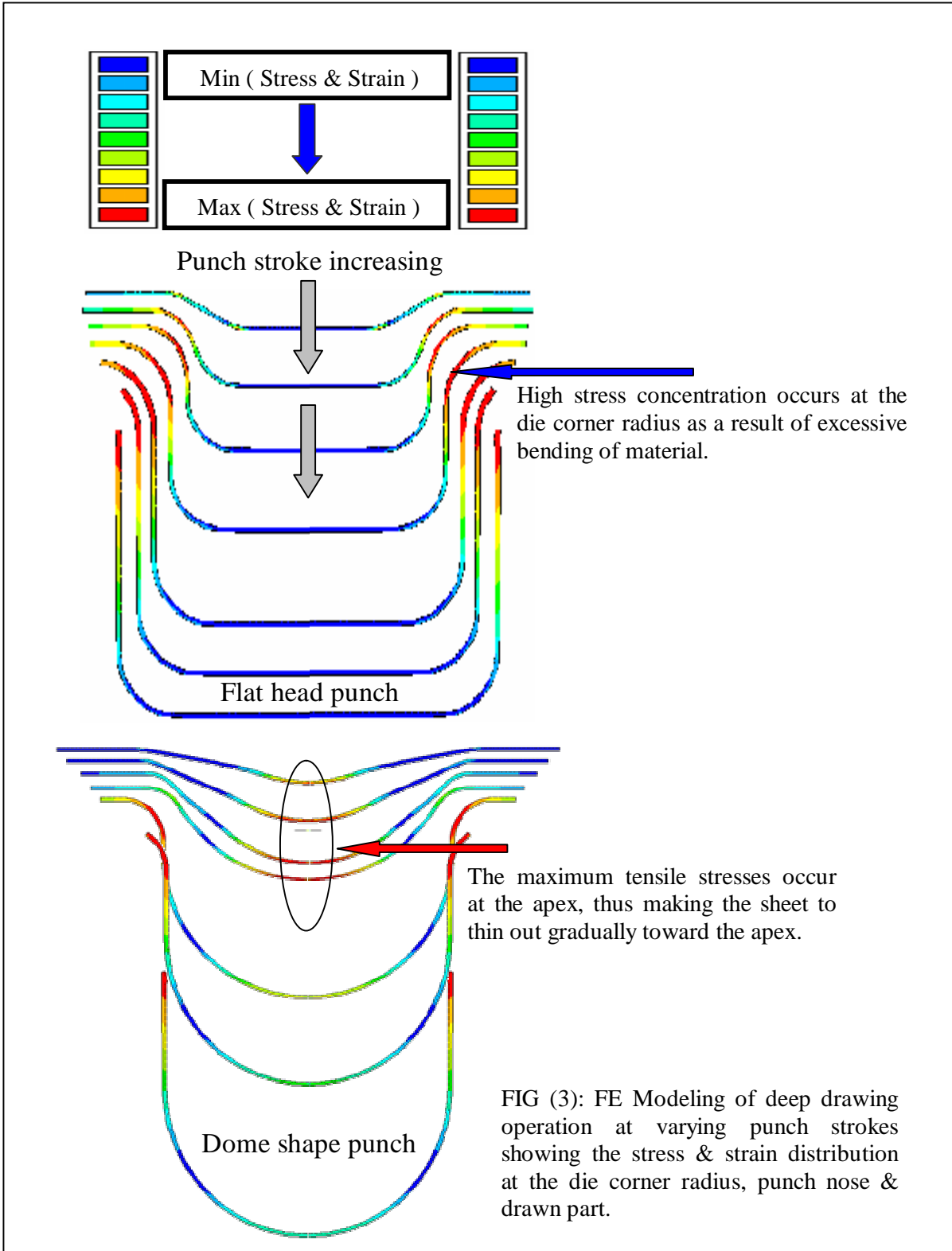


FIG (3): FE Modeling of deep drawing operation at varying punch strokes showing the stress & strain distribution at the die corner radius, punch nose & drawn part.

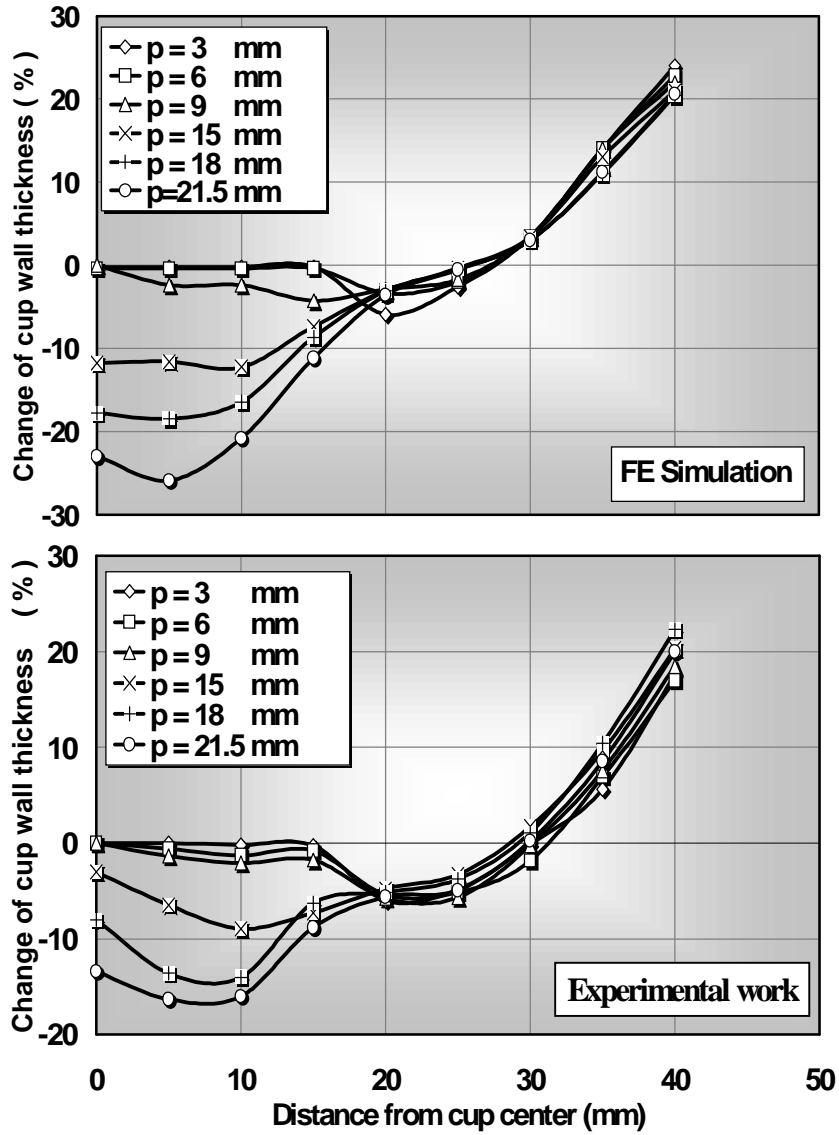


FIG (4): The effect of punch nose radius (P) on the cup wall thickness (Comparison between FEM & experimental work)

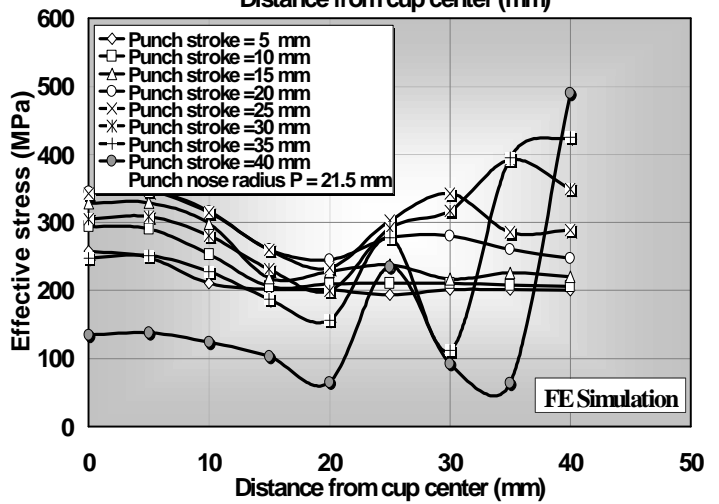
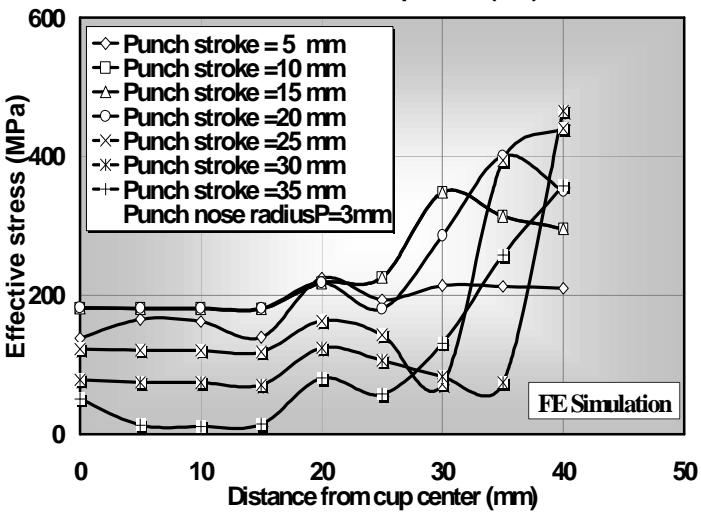
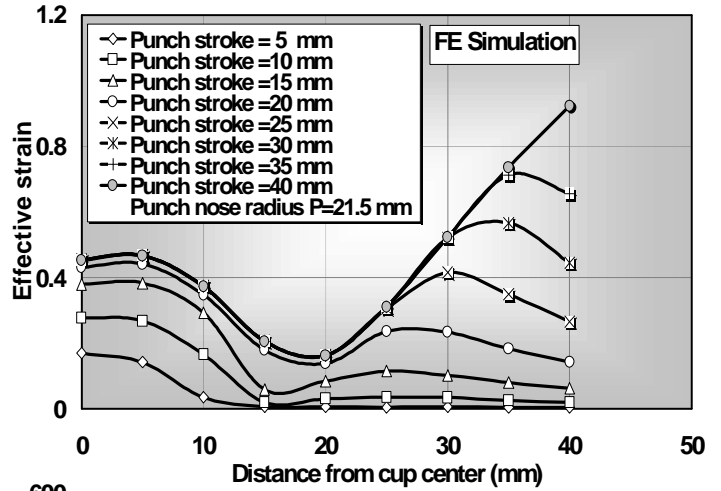
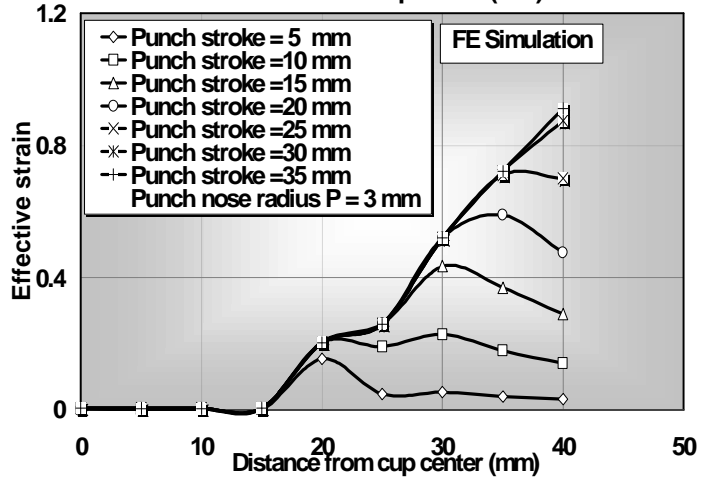
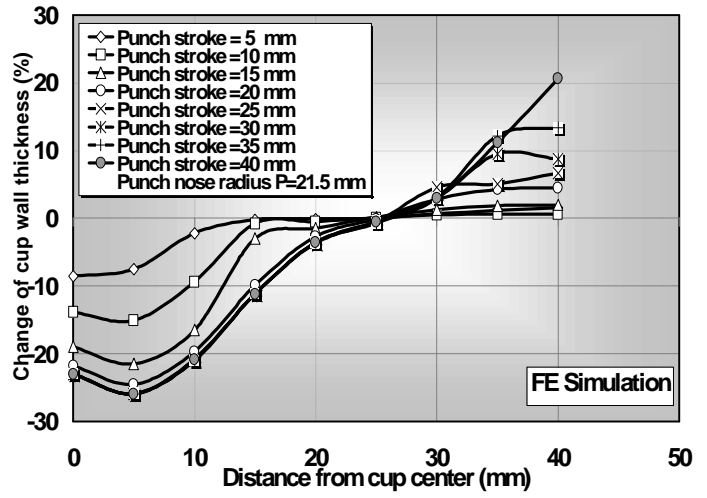
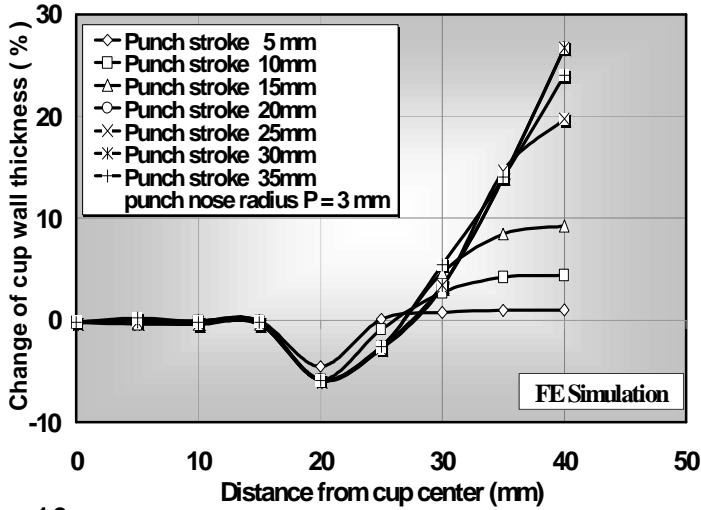


FIG (5): The effect of varying punch stroke on the cup wall thickness, stress and strain distribution over the cup wall.

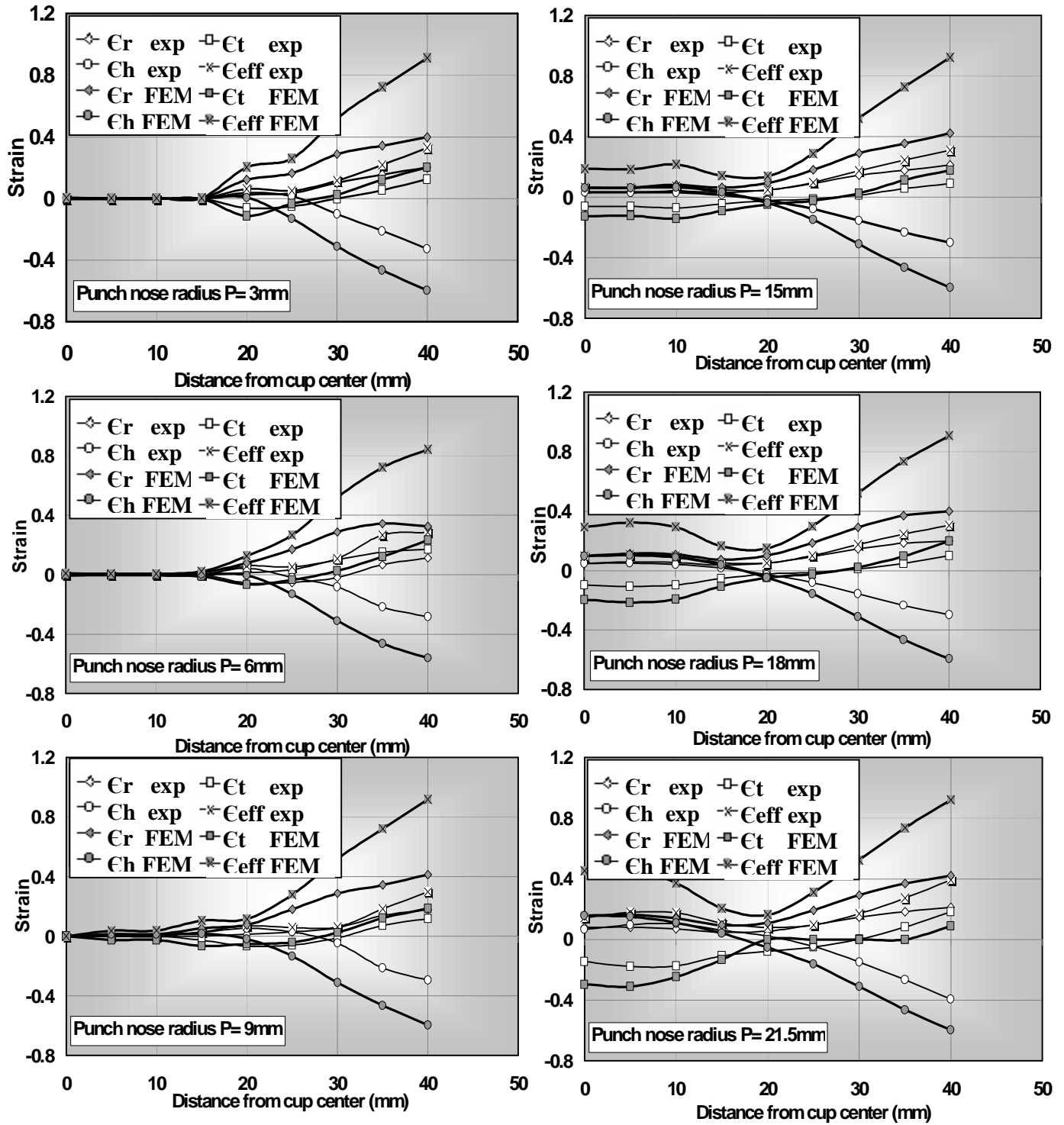


FIG (6): The effect of punch nose radius (P) on strain distribution over the cup wall. (Comparison between FEM & experimental work)

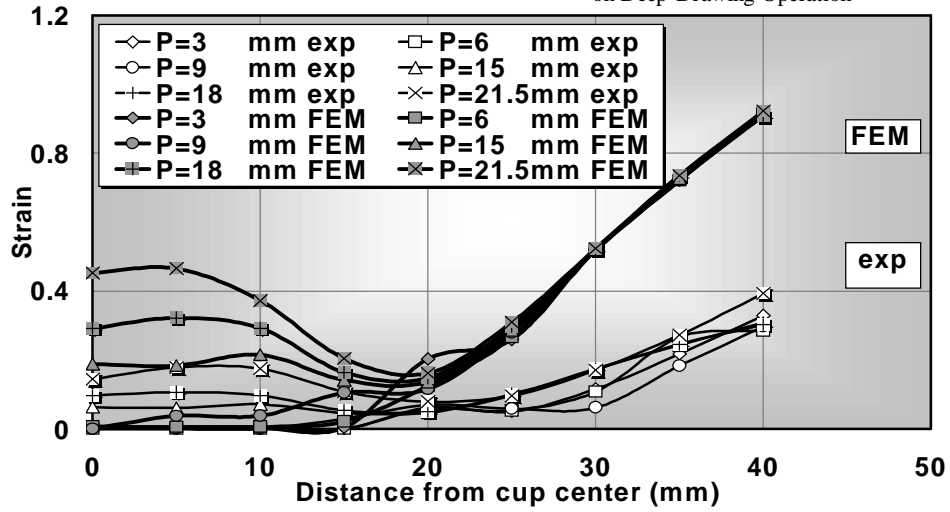


FIG (7): The effect of punch nose radius (P) on effective strain distribution over the cup wall (Comparison between FEM & Experimental work)

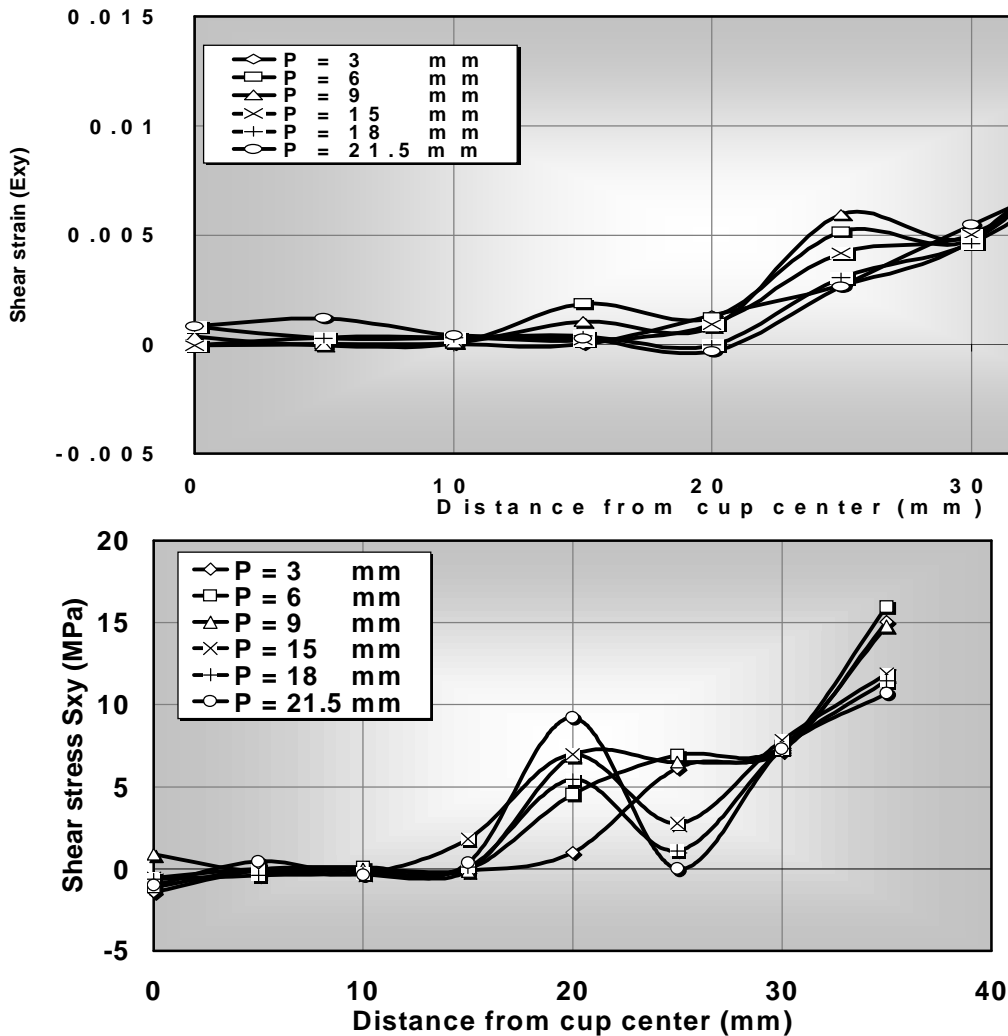


FIG (8): The effect of punch nose radius (P) on shear strain & shear stress distribution over the cup wall

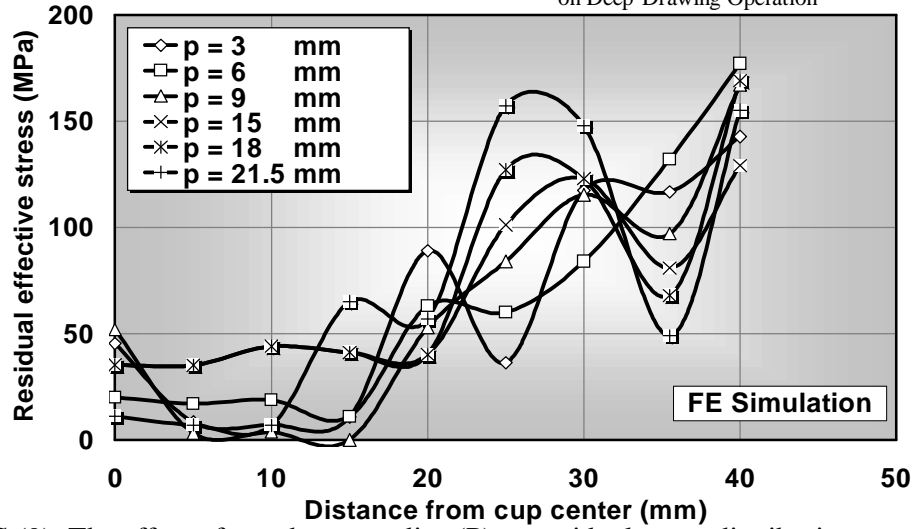


FIG (9): The effect of punch nose radius (P) on residual stress distribution over the cup wall

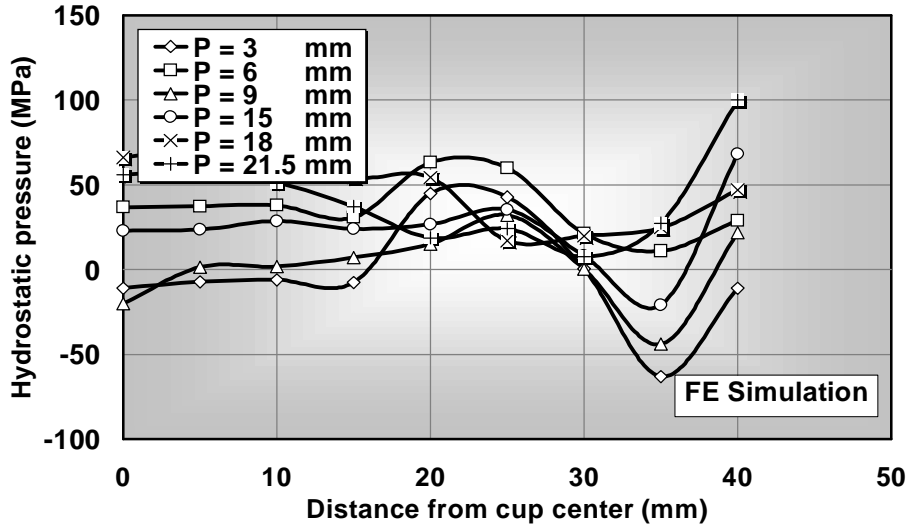


FIG (10): The effect of punch nose radius (P) on hydrostatic pressure distribution over the cup wall

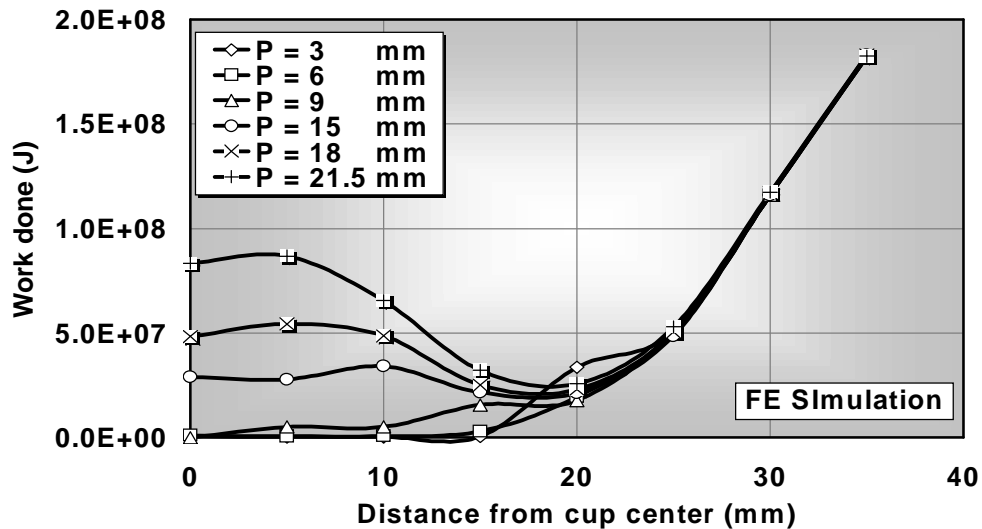


FIG (11): The effect of punch nose radius (P) on work done distribution over the cup wall